Surface selectivity in four-wave mixing: transient gratings as a theoretical and experimental example

I. M. Fishman

W. W. Hansen Experimental Physics Laboratory, Stanford University, Stanford, California 94305

C. D. Marshall, J. S. Meth,* and M. D. Fayer

Department of Chemistry, Stanford University, Stanford, California 94305

Received January 14, 1991; revised manuscript received May 16, 1991

A theoretical treatment of transient grating diffraction is derived for gratings that are spatially nonuniform in the direction perpendicular to the sample surface. This treatment is readily generalized to any four-wave mixing experiment. Both reflection and transmission geometries of diffraction are examined for the standard transient grating case, in which both grating excitation beams are incident upon the same side of the sample. For samples in which the grating amplitude perpendicular to the sample surface varies slowly relative to the optical wavelength, the reflection geometry is shown to probe only the surface or the interface, while the transmission geometry probes the bulk of the sample. An experimental example using four transient grating geometries (two reflection, two transmission) is shown to yield significantly different temporal responses, illustrating the nature of the theoretical predictions. The sample is a thin molecular crystal upon a substrate. Both electronic excitations (excitons) and wave-guided acoustic modes are generated and probed. Distinct signals are obtained from the bulk, the crystal–substrate interface, and the free-crystal face. Model calculations are presented that illuminate the behavior of the experimental example.

1. INTRODUCTION

Four-wave mixing experiments, which have expanded in areas of application and in sophistication over the past decade, have been successfully applied to the investigation of a wide variety of transient processes in liquids, solids, and gases. For example, transient gratings[1] were used to measure rotational diffusion rates in various liquids[2,3] and liquid crystals.[4] In addition, nonlinear [$\chi^{(3)}$] line shapes,[5] time-domain dynamics of optical phonons,[6] and vibrational relaxation rates in proteins[7] have been determined. Studies of solid systems have deduced the polariton diffusion constants in organic crystals[8] and the elastic constants of mineral extracts.[9] Gas-phase studies in flames have led to the measurement of radical ion concentrations[10] and collisional diffusion constants.[11] Other four-wave mixing techniques such as photon echos have provided insight into the coherence time for crystals,[12,13] glasses,[14,15] and semiconductor layer quantum wells.[16,17]

Previous research that utilizes nonlinear-optical techniques to study surfaces has concentrated on $\chi^{(2)}$ effects such as second-harmonic generation.[18] For a material that has inversion symmetry, second-harmonic generation is forbidden in the bulk of the material, but at the surface there is a break in the symmetry that permits a signal to be generated. Some other surface nonlinear-optical research has been performed that uses $\chi^{(3)}$ phenomena.[18] All these techniques have utilized geometries—such as surface plasmon waves and total internal reflection—that confine both the input and the signal electromagnetic waves to the surface region. These techniques are not generally practical for many experimental situations. The theory derived in this paper is fundamentally different. Transient gratings (and other four-wave mixing techniques) are essentially $\chi^{(3)}$ effects. In the ordinary transmission geometry, there is in general a signal from both the surface and the bulk, which, since they are degenerate in both time and propagation direction, cannot be distinguished from each other. When one considers the reflection signal geometry, a significantly different picture emerges. Owing to phase-matching considerations, there is no backward or reflection signal generated in the bulk of the material. The surface, however, produces a reflection signal that arises from the boundary conditions for electromagnetic waves.

Previous theoretical treatments of transient gratings[19] were developed by direct analogy with the diffraction for transparent volume holograms,[20,21] where the general method of slowly varying amplitudes was utilized. The grating was assumed to be constant in amplitude throughout the sample, and the probe beam was assumed to be weakly absorbed. This leads to a situation in which the diffracted light field amplitude builds up linearly with the length of the sample. Recent experimental investigations on samples with high optical densities,[22,23] e.g., metals and absorbing dielectrics with spatially nonuniform gratings, demonstrated that further theoretical development is required in which the effects of surfaces are included. Since it includes a position-dependent grating dielectric constant, the formalism presented here specifically considers, for the first time to our knowledge, the spatial origin of the transmission and reflection signals. This paper provides such a formalism for describing both reflection and transmission geometries of diffraction in which surface effects are specifically considered for samples with or without a high optical density and an arbitrary grating excitation profile.

0740-3224/91/091880-09$05.00 © 1991 Optical Society of America

Both the transmission and the reflection geometries utilized in this paper use the same grating orientation, in which the grating wave vector is perpendicular to the surface normal. This is the geometry that is used in a majority of transient grating experiments. It should be noted that the reflection geometry discussed in this paper differs from that normally discussed in the holography literature.[20] The formalism is developed in detail for both the transmission and the reflection geometries.

In the transmission geometry, when the sample is thick relative to the probe wavelength the signal is generated primarily as the probe passes through the bulk of the sample. For high optical densities at the probe wavelength, the probe is severely attenuated as it transits the sample. Nonetheless, it is shown that, when the grating amplitude is uniform inside the sample, the signal has identical contributions throughout the entire depth of the sample. For a grating that is nonuniform the signal field amplitude has contributions that are proportional to the grating amplitude at any point in the sample, regardless of the probe attenuation. The signal therefore properly represents the local diffraction efficiency, independent of the fact that the probe is attenuated by passing through the sample.

In the reflection geometry it is demonstrated that the signal arises from the surface (or incident interface) of the sample, provided that there is a grating modulation of the dielectric constant at the surface, an abrupt discontinuity of the dielectric constant at the surface, and slow changes (relative to the optical wavelength) in the grating amplitude perpendicular to the sample surface. This will always be the case for a weakly absorbing or nonabsorbing[24] condensed-matter sample with a surface in air or vacuum. The only limitation to the surface selectivity in this case is the depth of the abrupt discontinuity in the dielectric function. In general, this occurs on an atomic or molecular distance scale (1–10 Å).

When the absorption depths of the grating excitation and probe beams are of the order of an optical wavelength or less (high optical density), the slowly varying grating amplitude approximation does not apply. The reflection geometry is no longer surface selective, but rather it probes a depth into the sample that is comparable with the optical absorption (Beer's) length. This is in some sense counterintuitive. The weakly absorbing sample gives surface selectivity, while the strongly absorbing sample gives a signal from a significant depth into the sample. This allows for an interesting set of experiments. Surface-selective experiments can be performed far down the edge of an intense absorption band, where the optical density is low. As the light is tuned well into the absorption band and Beer's length is decreased to the order of a wavelength, the sampling depth is increased substantially. Such experiments would provide for a smooth transition from the observation of bulk phenomena to surface phenomena, which in turn would give information on the spatial extent of the surface properties of materials. Thus the reflection geometry can provide information on the properties of surface and interfacial regions, in contrast to the transmission geometry, which measures the mean bulk properties.

The surface selectivity is illustrated with experimental results from a thin anthracene crystal upon a fused-silica substrate that is excited and probed near the first polariton stop band. Data taken in the reflection geometry from the free (air–anthracene) interface and the bound (anthracene–glass) interface differ dramatically from the bulk measurements made in transmission. In addition, data taken in the reflection geometry from the free and the bound interfaces significantly differ from each other. The transient grating method can therefore directly and simultaneously provide information on the surface and bulk properties of a material.

2. THEORY

Consider a slab of material with the dielectric constant periodically modulated in the z direction, as shown in Fig. 1. If absorption is significant, one can neglect the effect of specular reflection from the back side of the sample. It is a straightforward extension of the following treatment to include the back-surface specular reflection if necessary. Treating only one interface is equivalent to considering a half-space of modulated material. The dielectric function has the form

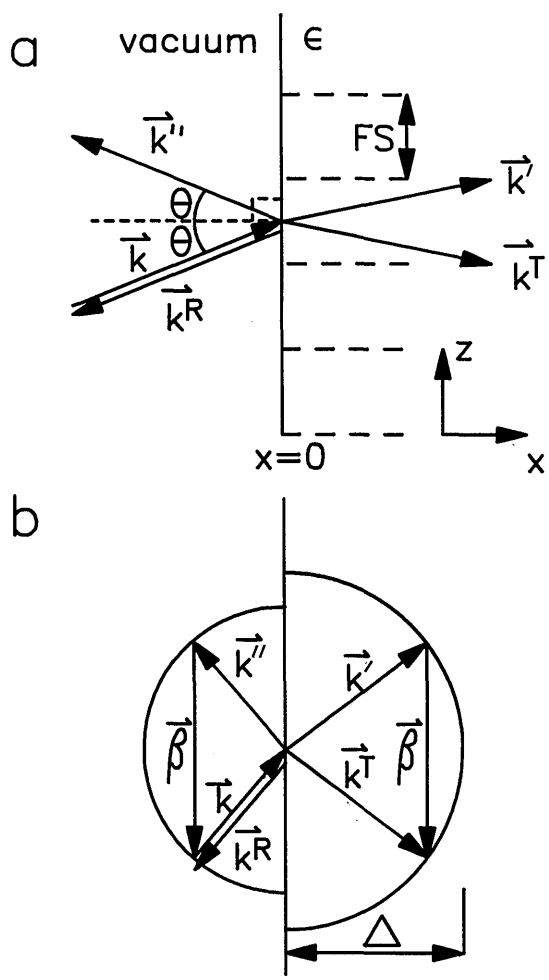

Fig. 1. a, The transient grating geometry for transmission and reflection diffraction geometries. The wave vectors of the incident probe, the reflected probe, the refracted probe, the reflected diffracted beam, and the transmitted diffracted beam are denoted $\mathbf{k}$, $\mathbf{k}''$, $\mathbf{k}'$, $\mathbf{k}^R$, and $\mathbf{k}^T$, respectively. The fringe spacing and the Bragg angle are denoted FS and θ, respectively. b, The wave-vector matching diagram. The grating wave vector is denoted β, and $\Delta = 2\pi\epsilon/\lambda$.

$$\epsilon(x, z) = \epsilon_0[\epsilon + \Delta\epsilon(x)\cos(\beta z)], \tag{1}$$

where ϵ_0 is the permittivity of free space. The unperturbed-material dielectric constant is denoted ϵ, $\Delta\epsilon(x)$ represents the spatially nonuniform grating amplitude perpendicular to the sample surface, and β is the grating wave vector, defined as $2\pi/\Lambda$, where the grating fringe spacing is

$$\Lambda = \lambda_{exc}/2 \sin\theta. \tag{2}$$

The two grating excitation beams have a wavelength λ_{exc} and cross at an angle 2θ; both the angle and the wavelength are measured outside the sample. It is convenient to present $\Delta\epsilon(x)/\epsilon$ as the product of a normalized function, which represents the spatial nonuniform excitation of the grating, and an amplitude p_0:

$$\Delta\epsilon(x)/\epsilon = p_0 P(x). \tag{3}$$

Starting with the wave equation for the E-field component of the electromagnetic field,[25]

$$-\nabla^2\mathbf{E} + \frac{\epsilon(x, z)}{c^2}\frac{\partial^2\mathbf{E}}{\partial t^2} = 0, \tag{4}$$

we obtain, after substitution of $\mathbf{E} = E\exp(-i\omega t)$ and incorporation of the dielectric function given by Eqs. (1) and (3),

$$\frac{\partial^2 E}{\partial x^2} + \frac{\partial^2 E}{\partial z^2} + \frac{\omega^2\epsilon_0\epsilon}{c^2}[1 + p_0 P(x)\cos(\beta z)]E = 0. \tag{5}$$

For $p_0 \ll 1$, which corresponds to the weak-diffraction limit, only the first order of diffraction needs to be considered. This is a reasonable assumption, since a typical transient grating experiment would have $p_0 \leq 0.01$. The solution to Eq. (5) is represented as an expansion in powers of p_0:

$$E = u_0(x)\exp(i\mathbf{k}_z' z) + (1/2)p_0 u_1(x) \times \{\exp[i(\mathbf{k}_z' + \beta)z] + \exp[i(\mathbf{k}_z' - \beta)z]\} + \ldots. \tag{6}$$

Substitution of Eq. (6) into Eq. (5) leads, to first order in p_0, to the following equations for the fundamental field u_0 and the first-order diffracted field u_1:

$$\frac{d^2 u_0}{dx^2} + \left(\frac{\omega^2\epsilon}{c^2} - \mathbf{k}_z^2\right)u_0 = 0, \tag{7a}$$

$$\frac{d^2 u_1}{dx^2} + \left[\frac{\omega^2\epsilon}{c^2} - (\mathbf{k}_z + \beta)^2\right]u_1 = \frac{\omega^2\epsilon}{c^2}P(x)u_0. \tag{7b}$$

Equation (7a) governs reflection and refraction of the fundamental probe wave according to the Fresnel relations. Equation (7b) describes the amplitude of the diffracted wave in vacuum [$x < 0$, $\epsilon = 1$, and $P(x) \equiv 0$] and in the media ($x > 0$). The right-hand side of Eq. (7b) is the source term that transfers the fundamental wave amplitude into the first diffracted order. Since the diffraction is weak, coupling of the diffracted beam back into the fundamental has been ignored, which led to the right-hand side of Eq. (7a) being set equal to zero.

One can recognize that Eqs. (7a) and (7b) are almost identical to the system of equations used by Bloembergen[26] for the description of parametric interaction of optical waves on the boundary of nonlinear media. The only difference is in the x-coordinate dependence of the excitation or coupling term $P(x)$. The solution of Eq. (7a) is

$$u_0 = \exp(i\mathbf{k}_x x) + A_R\exp(-i\mathbf{k}_x'' x) \quad (x < 0), \tag{8a}$$

$$u_0 = A_T\exp(i\mathbf{k}_x' x) \quad (x > 0), \tag{8b}$$

where A_R and A_T are the amplitudes of the reflected and transmitted waves, respectively, as determined by the Fresnel relations. The incident E field has been set to unity. The x components of the wave vectors $\mathbf{k}$ and $\mathbf{k}''$ of the fundamental incident and reflected waves and $\mathbf{k}'$ of the fundamental transmitted wave are given by

$$\mathbf{k}_x^2 = \mathbf{k}_x''^2 = \omega^2/c^2 - \mathbf{k}_z^2, \tag{9a}$$

$$\mathbf{k}_x'^2 = \epsilon\omega^2/c^2 - \mathbf{k}_z^2, \tag{9b}$$

where $|\mathbf{k}_z| = (\omega/c)\sin\theta$. For a graphic representation of the wave-vector relationships see Fig. 1.

Limiting ourselves to the case of TE polarization (electric vector perpendicular to the plane of incidence) and using the Maxwell boundary conditions for electric fields, which reduce to the continuity of u_0 and du_0/dx at $x = 0$, we obtain the Fresnel relations

$$A_R = \frac{\mathbf{k}_x'' - \mathbf{k}_x'}{\mathbf{k}_x'' + \mathbf{k}_x'}, \qquad A_T = \frac{2\mathbf{k}_x''}{\mathbf{k}_x'' + \mathbf{k}_x'}. \tag{10}$$

Introducing Eqs. (8) and (10) into Eq. (7b), one obtains the equation for the first-order diffracted field:

$$\frac{d^2 u_1}{dx^2} + \mathbf{k}_x^{*2}u_1 = \phi(x)\exp(i\mathbf{k}_x' x), \tag{11}$$

where $\mathbf{k}_x^*$ is the x component of the wave vector of either the transmitted or the reflected diffracted field. The wave vector of the transmitted diffracted field is given by

$$(\mathbf{k}_x^T)^2 = [\omega^2\epsilon/c^2 - (\mathbf{k}_z + \beta)^2] \quad (x > 0). \tag{12a}$$

The wave vector for the reflected diffracted wave is

$$(\mathbf{k}_x^R)^2 = [\omega^2/c^2 - (\mathbf{k}_z + \beta)^2] \quad (x < 0), \tag{12b}$$

and the coupling parameter is denoted as

$$\phi(x) = P(x)A_T\omega^2\epsilon/c^2. \tag{12c}$$

The solution of Eq. (11) may be written in the form

$$u_1(x) = a_R\exp(i\mathbf{k}_x^R x) \quad (x < 0), \tag{13a}$$

$$u_1(x) = a_T\exp(i\mathbf{k}_x^T x) + \frac{1}{2i\mathbf{k}_x^T} \times \int_0^\infty \exp(i\mathbf{k}_x^T|x - x'|)\phi(x')\exp(i\mathbf{k}_x' x')dx' \quad (x > 0), \tag{13b}$$

where $(1/2i\mathbf{k}_x^T)\exp(i\mathbf{k}_x^T|x - x'|)$ is the Green function of Eq. (11). We determine the amplitudes of the transmitted and reflected diffracted waves, denoted a_T and a_R, respectively, by matching the boundary conditions for the tangential components of the electric and magnetic fields, which reduce again to the continuity of u_1 and du_1/dx at $x = 0$. Keeping in mind that $|x - x'| \equiv x' - x$ for the case of interest, one obtains the following equations from

the boundary conditions of Eq. (13):

$$a_R = a_T + M, \tag{14a}$$

$$-k_x{}^R a_R = \mathbf{k}_x{}^T(a_T - M), \tag{14b}$$

where

$$M = \frac{1}{2i\mathbf{k}_x{}^T}\int_0^\infty \exp[i(\mathbf{k}_x{}^T + \mathbf{k}_x')x']\phi(x')\mathrm{d}x'. \tag{14c}$$

Solving and substituting Eqs. (14) into Eqs. (13) provide the final result for the fields:

$$u_1{}^R(x) = \frac{-i\exp(i\mathbf{k}_x{}^R x)}{\mathbf{k}_x{}^T + \mathbf{k}_x{}^R} \times \int_0^\infty \exp[i(\mathbf{k}_x{}^T + \mathbf{k}_x')x']\phi(x')\mathrm{d}x' \quad (x < 0) \tag{15a}$$

for the reflection geometry and

$$u_1{}^T(x) = \frac{\mathbf{k}_x{}^T - \mathbf{k}_x{}^R}{\mathbf{k}_x{}^T + \mathbf{k}_x{}^R}\exp(i\mathbf{k}_x{}^T x)M + \frac{1}{2i\mathbf{k}_x{}^T}\int_0^\infty \exp(i\mathbf{k}_x{}^T|x - x'|)\exp(i\mathbf{k}_x'x')\phi(x')\mathrm{d}x' \quad (x > 0) \tag{15b}$$

for the transmission geometry.

The general solution for the reflected diffracted wave can be simplified by substitution of

$$\mathbf{k}_x{}^T = \mathbf{k}_x', \tag{16}$$

which is valid for Bragg's condition (see Fig. 1b). For the case of a slowly varying dielectric modulation [$\phi(x)$] in the x direction relative to the optical wavelength, the second derivative $\mathrm{d}^2\phi(x)/\mathrm{d}x^2$ can be neglected. After double partial integration of Eq. (15a) one obtains

$$u_1{}^R(x < 0) \simeq \exp(-i\mathbf{k}_x{}^R x)\left[\frac{(\phi)_{x=0}}{(\mathbf{k}_x{}^T + \mathbf{k}_x{}^R)(\mathbf{k}_x{}^T + \mathbf{k}_x')} + \frac{i(\mathrm{d}\phi/\mathrm{d}x)_{x=0}}{(\mathbf{k}_x{}^T + \mathbf{k}_x{}^R)(\mathbf{k}_x{}^T + \mathbf{k}_x')^2} + \cdots\right] \tag{17}$$

for the amplitude of the reflected diffracted wave. Relation (17) shows that if the modulation function is approximately constant and changes only gradually ($\phi \simeq$ constant and $\mathrm{d}\phi/\mathrm{d}x \ll \mathbf{k}''$), then the diffracted wave amplitude comes entirely from the first term on the right-hand side of relation (17), which coincides with Bloembergen's result[26] for parametric amplification.

For the amplitude of a transmitted wave, given by Eq. (15b), the limiting case described above for reflection produces the result

$$u_1{}^T(x > 0) = \exp(i\mathbf{k}_x{}^T x)\left[a_R + \frac{1}{2i\mathbf{k}_x{}^T}\int_0^T \phi(x')\mathrm{d}x'\right], \tag{18}$$

where a_R is the amplitude of the reflected diffracted wave as defined by Eqs. (14). The position in the sample at which the diffraction is measured is denoted T. Alternatively, if the sample is a slab and the transmitted diffraction is measured outside the sample, the thickness of the slab is T. As one would expect, the transmitted diffracted wave amplitude is proportional to the sample thickness [if $\phi(x)$ = constant] plus the surface contribution a_R. It should be noted that the theory derived above is not rigorously valid for a slab that has two interfaces. However, for a sample that has a high optical density one can neglect the effects of the second interface, since the fields are weak there. Otherwise, an analogous treatment can be used for the second interface.

Using Eq. (15a), one can obtain a general expression for the reflected diffraction efficiency at the Bragg angle of the probe light intensity,

$$\eta^R = \frac{\omega^2}{c^2}\frac{\cos^2\theta}{(\cos\theta + \sqrt{\epsilon - \sin^2\theta})^4} \times \left|\int_0^T \exp[2i(\omega/c)\sqrt{\epsilon - \sin^2\theta}x']\Delta\epsilon(x')\mathrm{d}x'\right|^2, \tag{19}$$

which is reduced with the use of relation (17), for slowly varying $\Delta\epsilon(x)$, i.e., $\mathrm{d}\Delta\epsilon/\mathrm{d}x \ll \epsilon^{1/2}/\lambda$, inside the sample, to

$$\eta^R = \left|\frac{(\cos\theta)(\Delta\epsilon)_{x=0}}{2\sqrt{\epsilon - \sin^2\theta}(\cos\theta + \sqrt{\epsilon - \sin^2\theta})^2}\right|^2 + \left|\frac{(\cos\theta)(\mathrm{d}\Delta\epsilon/\mathrm{d}x)_{x=0}}{4(\omega/c)(\epsilon - \sin^2\theta)(\cos\theta + \sqrt{\epsilon - \sin^2\theta})^2}\right|^2, \tag{20}$$

where $(\Delta\epsilon)_{x=0}$ and $(\mathrm{d}\Delta\epsilon/\mathrm{d}x)_{x=0}$ are the magnitudes at the interface ($x = 0$) of the modulated component of the dielectric function and its x derivative, respectively.

The general expression for the diffraction efficiency of the transmitted wave for a slab of thickness T at the Bragg angle, which is derived from Eq. (15b), yields

$$\eta^T = \frac{\omega^2\cos^2\theta\exp(-\Omega T)}{4c^2|\sqrt{\epsilon - \sin^2\theta}(\cos\theta + \sqrt{\epsilon - \sin^2\theta})|^2} \times \left|\frac{\cos\theta - \sqrt{\epsilon - \sin^2\theta}}{\cos\theta + \sqrt{\epsilon - \sin^2\theta}} \times \int_0^T \exp[2i(\omega/c)\sqrt{\epsilon - \sin^2\theta}x']\Delta\epsilon(x')\mathrm{d}x' + \int_0^T \Delta\epsilon(x')\mathrm{d}x'\right|^2 \tag{21}$$

and is reduced in the limit of slowly varying $\Delta\epsilon(x)$ to

$$\eta^T = \frac{\cos^2\theta\exp(-\Omega T)}{4|\sqrt{\epsilon - \sin^2\theta}(\cos\theta + \sqrt{\epsilon - \sin^2\theta})|^2} \times \left|\frac{\cos\theta - \sqrt{\epsilon - \sin^2\theta}}{\cos\theta + \sqrt{\epsilon - \sin^2\theta}}\frac{(\Delta\epsilon)_{x=0}}{2i\sqrt{\epsilon - \sin^2\theta}} + \frac{\omega}{c}\int_0^T \Delta\epsilon(x')\mathrm{d}x'\right|^2, \tag{22}$$

where $\Omega T = D(\ln 10)/\cos\theta$, which accounts for Beer's law attenuation of the probe beam, and D is the optical density. The first term in the modulus on the right-hand sides of these equations is the surface contribution for the incident interface ($x = 0$). The second term is the bulk contribution, which will dominate for samples thicker than $\sim\lambda\epsilon^{-1/2}$. Equations (19)–(22) are strictly valid only when the reflections from the second interface ($x' = T$) can be neglected. Experimentally, this can be realized in

several ways; e.g., in an optically dense sample the light fields are significantly attenuated at the second interface of the slab ($x' = T$), and in a thick sample the grating excitation beams do not cross at the second interface.

All the preceding expressions are correct for the case of a complex dielectric constant in an absorbing medium. The dielectric constant ϵ is explicitly replaced by

$$\tilde{\epsilon} = \epsilon' + i\epsilon'', \tag{23}$$

and all the wave vectors are replaced by the appropriate complex wave vectors. Starting with a complex index of refraction, $\tilde{n}_0$, that is weakly modulated with the grating periodicity gives

$$\tilde{n}(x,z) = \tilde{n}_0 + \Delta\tilde{n}(x,z) = (n_0' + in_0'') + \cos(\beta z)[\Delta n'(x) + i\Delta n''(x)]. \tag{24}$$

Ignoring terms that are second order in Δ leads to the grating dielectric amplitude

$$\Delta\tilde{\epsilon}(x) = 2\tilde{n}_0[\Delta n'(x) + i\Delta n''(x)]. \tag{25}$$

The substitution of Eq. (25) into Eq. (22) after the surface term is dropped leads to the bulk contribution of the transmitted diffraction efficiency for a slab of thickness T:

$$\eta = \exp(-\Omega T)\frac{\omega^2|\tilde{n}_0|\cos^2\theta}{c^2|\sqrt{\epsilon - \sin^2\theta}(\cos\theta + \sqrt{\epsilon - \sin^2\theta})|^2} \times \left|\int_0^T [\Delta n'(x') + i\Delta n''(x')]\mathrm{d}x'\right|^2. \tag{26}$$

Treating $\Delta n'$ and $\Delta n''$ as constants and setting $|\tilde{n}_0| \simeq 1$ lead to the well-known result for transmitted diffraction in the weak-diffraction limit[19–21]:

$$\eta^T = \exp(-\Omega T)\left(\frac{\pi T}{\lambda\cos\theta}\right)^2(\Delta n'^2 + \Delta n''^2). \tag{27}$$

3. DISCUSSION

The most important aspect of Section 2 is the surface-sensitive nature of the reflected diffraction signal given by Eq. (20). As in surface second-harmonic generation, only the surface region is probed with the reflected diffraction experiment if the modulation function has an abrupt change at the interface and changes gradually inside the material [$\Delta\epsilon \gg (\mathrm{d}\Delta\epsilon/\mathrm{d}x)\mathbf{k}'^{-1}$]. For many experimental situations the $(\Delta\epsilon)_{x=0}$ (offset) term dominates. If $\mathrm{d}\Delta\epsilon/\mathrm{d}x$ is large, i.e., the index modulation is rapidly varying relative to the probe wavelength, then higher-order terms need to be considered, and the signal may have some bulk contribution created by the rapid index changes inside the material.

The transmitted diffraction experiment is significantly different. The signal has a surface contribution that is identical to that of the reflection case, but there is also a contribution from the bulk of the material. If the material is thick relative to the wavelength of the probe inside the sample ($\lambda\epsilon^{-1/2}$), then the surface term has negligible amplitude, assuming that the index modulation is of equal amplitude throughout the sample. On the other hand, if the sample is thin relative to the probe wavelength inside the sample, the reflection terms will dominate, and the bulk contribution to the signal will be small. The attenuations of the probe and diffracted beams as they propagate through the sample are equal, since the path length is a constant when the probe is incident at the Bragg angle. This leads to an equal spatial weighting of the contributions to the diffracted signal.

In the case of a thick sample with a slowly varying index modulation, the transmission case uniformly probes the bulk, while the reflection case probes only the surface. This leads to a new approach for observing both surface and bulk phenomena with the same transient grating experimental method. A similar formalism could be derived for different types of four-wave mixing experiments such as photon echoes. In this case modulation of the dielectric function is expressed with the use of the appropriate time-dependent polarization induced by the optical pulses.

4. EXPERIMENTAL EXAMPLE

In this section an experimental example is presented. The system, anthracene single crystals excited and probed near the first polariton stop band, is complex. Our purpose here is to illustrate the difference between transmission and reflection geometries without treating in detail the underlying complexities of the system. Furthermore, the model calculations will be significantly simplified to illustrate the diffraction phenomena rather than to reproduce the exact time dependence of the data.

A. Experimental Procedures

The output of a Q-switched, mode-locked Nd:YAG laser is frequency doubled to a wavelength of 532 nm and used to pump a red dye laser. A cavity-dumped pulse from the dye laser is frequency summed with a single infrared pulse from the Nd:YAG laser to produce a tunable near-UV source of 3-μJ, 30-ps pulses at a 600-Hz repetition rate. The UV pulse is then split into three pulses. Two pulses are crossed at an angle 2θ to produce a sinusoidal interference pattern in the sample. The wavelength of the laser is tuned so that the anthracene strongly absorbs the light, but there is still significant transmission owing to the thinness of the sample. Absorption of the light produces both electronic excitations and acoustic standing waves.[27] The third pulse is the probe and is incident from either the front or the back of the sample. The probe is temporally delayed and diffracted from the transient holographic grating in both transmission and reflection geometries. Four experimental probe geometries are sequentially observed under identical grating excitation conditions. These geometries consist of two transmission and two reflection configurations, as shown in Fig. 2. The two front probe geometries, in which the excitation and probe beams are incident upon the same interface, are shown in Fig. 2a. The two back probe geometries, in which the probe is incident upon the opposite interface, are depicted in Fig. 2b. The diffracted signal is detected with a photomultiplier tube and a lock-in amplifier. A computer is used to signal average many scans of the delay line to provide an improved signal-to-noise ratio. Experiments were performed on anthracene single crystals grown by sublimation. The samples were placed upon a glass optical flat oriented with the anthracene a–b plane

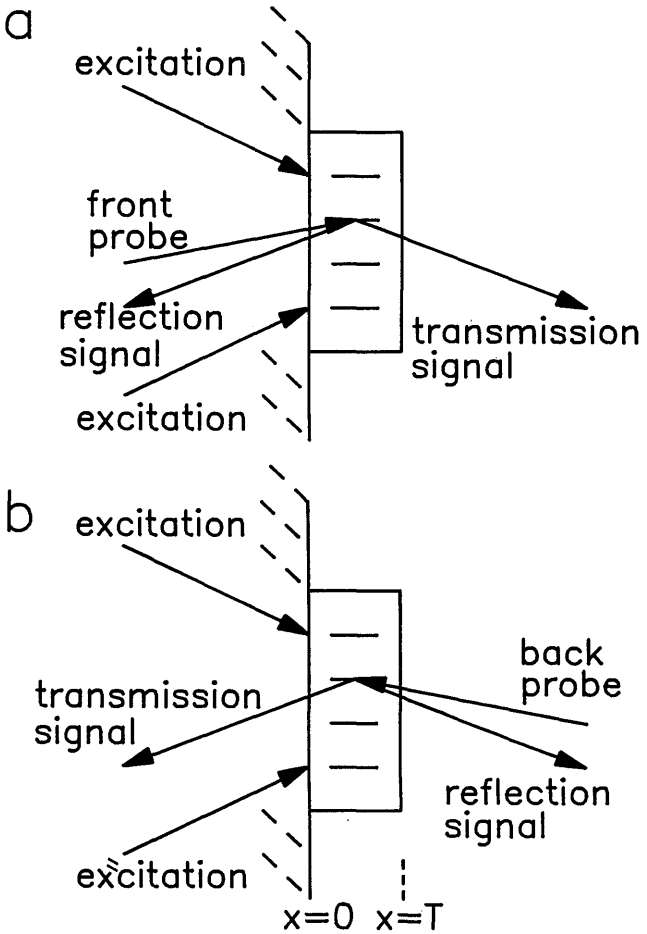

Fig. 2. Four transient grating experimental geometries used for Fig. 3; a and b are for a front (anthracene–substrate interface) and a back (anthracene–air interface) incident probe, respectively.

perpendicular to the surface normal of the substrate. The grating wave vector and the laser polarization were parallel to the *a* axis, and the grating excitation beams were incident upon the anthracene–glass interface. The sample, which is 350 nm thick, has an optical density of 0.38 at the laser wavelength of 398.6 nm, the red edge of the first absorption band. A detailed description of the sample preparation is provided elsewhere.[28]

B. Results and Discussion

Figure 3 shows the experimental results for the transient grating experiments on the four grating geometries in Fig. 2. The first two are transmission geometries with the probe beam incident upon either the anthracene–substrate interface (front; Fig. 3a) or the free (back; Fig. 3b) surface. The third and the fourth are reflection geometries with excitation incident upon the front (Fig. 3c) or the back (Fig. 3d) side of the sample. The complicated beating pattern seen in all the data sets arises from the acoustic waveguide nature of the thin samples.[28–30] Many different acoustic modes are excited inside the sample, which leads to a superposition of many different frequency components.

The transmission geometries give virtually identical signals, particularly in contrast with the two reflection cases. The excitation beams are substantially attenuated in passing through the sample. Therefore more excitations are produced near the front surface. The probe is also attenuated in passing through the sample. Nonetheless, the signal is the same whether the probe first encounters the regions of higher or lower excited-state density. The theory, which shows that diffraction for a transmission geometry has equal spatial weighting throughout the bulk of the sample, implies that the probe beam direction is irrelevant, in agreement with experimental observations. Minor differences between the two transmission data sets can arise from slight differences in alignment of the probe beam that occur in switching geometries and from the low-amplitude contributions from the surface component of the signal, which are not necessarily the same at the free surface and the anthracene–substrate interface.

The two reflection signals are fundamentally different from the transmission signals. The transmission signals (Figs. 3a and 3b) show a large, slowly decaying offset from the zero baseline. This is due to the generation of excited states (polaritons or possibly polaritons that have decayed into excitons) in the bulk. The offset decays only partially during the ~20 ns of data. Figure 3c shows reflection data taken from the crystal–substrate (incident grating excitation) interface. The offset decays rapidly,

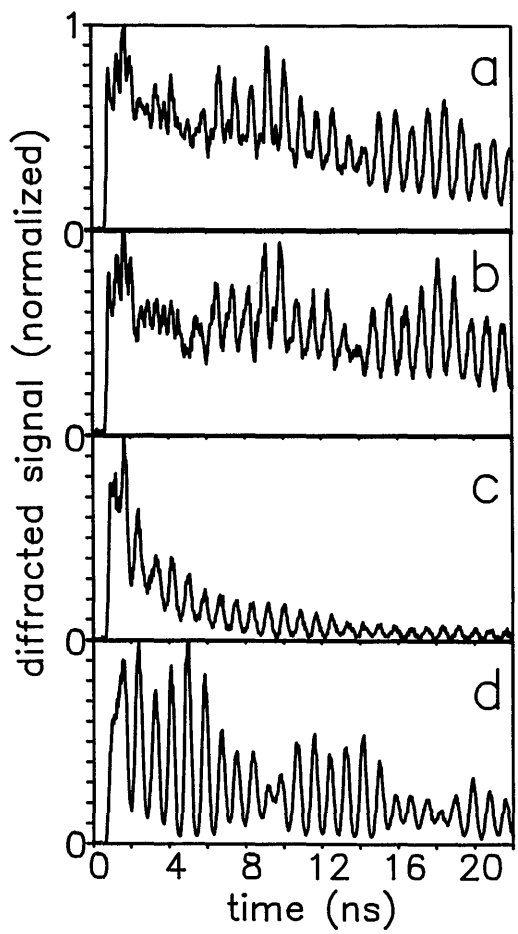

Fig. 3. Transient grating signals on 350-nm-thick anthracene crystals with an optical density of 0.38 at the experimental wavelength of 398.6 nm. a, b, The transmission geometry of diffraction with the probe beam incident upon the front (a) and the back (b) of the sample. c, d, The reflection geometry of diffraction and the probe incident upon the front and the back of the sample, respectively.

and the acoustic waves, which are modified by the presence of the interface, show a simple pattern. Figure 3d shows reflection data from the free crystal surface. The offset in signal caused by excited states is small, even at time $t = 0$. The beating pattern is again complex. Fourier transforms of the data show that Figs. 3a, 3b, and 3d have the same frequencies, consisting of five modes, while the crystal–substrate interface incident reflection signal displays only one of the frequencies.

For the reflection geometry, in which the probe is incident upon the crystal–substrate interface (Fig. 3c), the signal arises entirely from the interface of the sample, which contains a large population of the excited electronic states. The signal consequently shows a ratio of excited-state to acoustic contribution of approximately 2:1. For the case of a reflection geometry, in which a back incident probe is used (Fig. 3d), the ratio of the excited states to the acoustic contribution is approximately 1:2. This can be understood qualitatively, since the acoustic disturbance is more or less constant throughout the sample in the x dimension, while the excited states are exponentially weighted near the front (incident excitation side) of the sample owing to Beer's law absorption of the excitation beams. Since a reflected diffracted signal samples only the probe inci-dent interface, the signal that is derived from the back (opposite the incident excitation side) interface has a much larger acoustic, rather than excited-state, signal amplitude.

As is pointed out above, the excited-state decay characteristics also differ dramatically in the reflection-versus-transmission data. This can be understood from a consideration of the surface selectivity of the reflected diffraction signal. The reflection signal will probe surface excitations (surface polaritons). It is known that excitation transport in anthracene crystals at room temperature is slow on the experimental distance (~1 μm) and time (~10 ns) scales and that transport in the c crystallographic axis direction (approximately the surface-normal direction) is extremely slow. Therefore the surface states and the bulk states can decay at independent rates, and the surface states will not be significantly repopulated by diffusion of excitations from the bulk.

Clearly, the physical phenomena occuring in the anthracene crystal are complex. The object of the discussion given above is not to illustrate the details of the dynamical processes in anthracene but rather to illustrate that dramatic differences can be observed in a comparison of reflection and transmission geometries of diffraction. This is in accord with the theoretical development, which demonstrates that reflection and transmission signals probe distinct spatial regions of the sample.

C. Calculation Example

A calculation applying the theory developed in Section 2 that uses a simple physical model of the anthracene system can illustrate the same trends as those seen in the data. To demonstrate the theory, we retain only the essential physical features in the model. A single acoustic wave will be used rather than the multiple modes observed, and acoustic damping will not be included. Decay of the surface excited states and bulk excited states will be taken to be independent, with each characterized by a single exponential lifetime. For mixed excited-state and acoustic transient gratings studied to date, for small values of n'' ($n'' \ll 1$) the primary contributions to $\Delta n'$ and $\Delta n''$ can be written as[19]

$$\Delta n''_{ex}(x,t) = -[\Delta N_1(x,t)/N_0]n''_0(\omega), \tag{28a}$$

$$\Delta n'_{ex}(x,t) = -[\Delta N_1(x,t)/N_0]n''_0(\omega)2(\omega - \omega_0)/\Delta\omega, \tag{28b}$$

$$\Delta n'_{str}(x,t) = -\Delta S(x,t)(n_0'^2 - 1)/2n'_0, \tag{28c}$$

where $\Delta n''_{ex}$ and $\Delta n'_{ex}$ are the grating peak-to-null variations in the components of the complex index of refraction due to the presence of electronic excited states and $\Delta n'_{str}$ is the variation due to the presence of strain. The number density ratio of excited states to ground states in the grating peak to the null is $\Delta N_1(z,t)/N_0$. The peak-to-null difference in strain due to an acoustic disturbance is written as $\Delta S(z,t)$. The transition line width and the resonance frequency are written as $\Delta\omega$ and ω_0. The real and imaginary parts of the probe's unperturbed index of refraction are again written as n' and n''. The above contributions to $\Delta n'$ and $\Delta n''$, which are utilized as examples in this paper, are discussed in detail elsewhere.[19]

There are two possible mechanisms that could produce acoustic strain.[27] They are Brillouin scattering and heating due to radiationless relaxation of the excited states. The experimental data used in this paper do not provide enough information to permit us to distinguish between the two mechanisms. The Brillouin scattering mechanism will be assumed, since it leads to a brief theoretical description. The simplest expression for the lowest-order acoustic mode of an isotropic slab on a half-space (Rayleigh mode) is found in the limit of infinite fringe spacing[30] ($\beta = 0$) that will be used here. The strain in the sample due to the single lowest mode can now be written as

$$\Delta S(x,t) = \Delta S^0 n''_{exc} \sin(\omega_{ac} t), \tag{29}$$

where n''_{exc} and ω_{ac} are the imaginary portion of the index of refraction for the excitation beams and the acoustic frequency for the acoustic mode, respectively. Assuming a single exponential excited-state lifetime τ_b in the bulk of the slab and a surface lifetime τ_s, the excited-state distribution can be written as

$$\frac{\Delta N_1(x,t)}{N_0} = \Delta N^0 n''_{exc}(\omega)\exp(-\Omega x) \times \left[a(x)\exp\left(-\frac{t}{\tau_b}\right) + b(x)\exp\left(-\frac{t}{\tau_s}\right)\right], \tag{30}$$

where Beer's law is used to describe the spatial distribution of excited states generated by the grating excitation beams incident upon the $x = 0$ side of the sample. The bulk component amplitude $a(x)$ is equal to unity in the interval $0 < x < T$ and is equal to zero elsewhere. The surface component amplitude $b(x)$ is equal to unity at the interfaces ($x = 0, x = T$) and is zero elsewhere.

These initial grating conditions can be probed with four transient grating probe configurations discussed in Subsections 4.A and 4.B. The first two are transmission diffraction geometries from a probe incident upon either the front or the back side of the sample. The third and the fourth are reflected diffraction geometries with the probe incident upon the back or the front interface. Since the Beer length of the material is approximately two

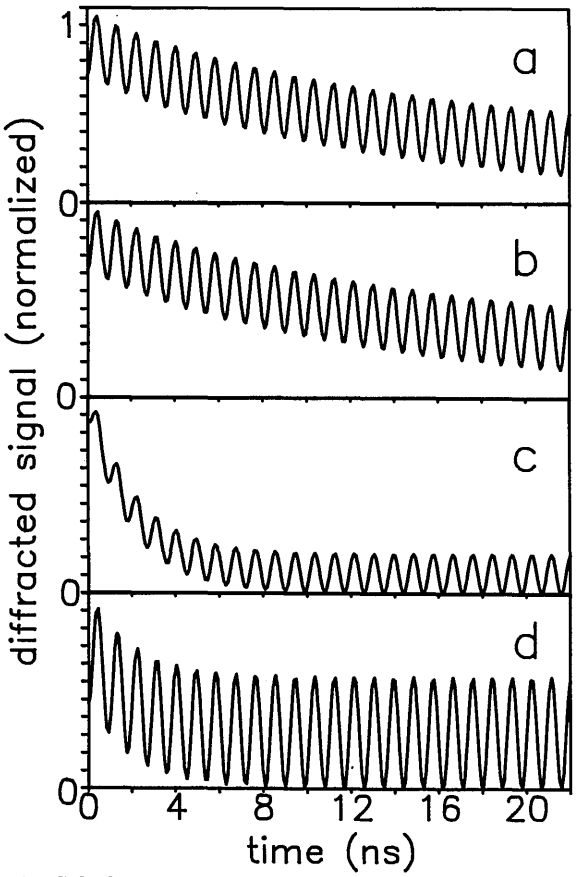

Fig. 4. Calculated transient grating signals for a mixed excited-state acoustic grating of a thin film. a, b, Front and back incident probes, respectively, in a transmission diffraction geometry. c, d, Front and back incident probes, respectively, with a reflection geometry of diffraction.

Table 1. Parameters Used in Fig. 4 to Model a Transient Grating Diffraction Efficiency

Sample thickness (T)	350 nm
Wavelength (λ)	398.6 nm
Acoustic angular frequency(ω_{ac})	3.49×10^9 rad/s
Detuning $[(\omega - \omega_0)/\Delta\omega]$	0.0
Optical density	0.38
Index of refraction ($n' + in''$)	$2.2 + i0.079$
Bragg angle (θ)	0°
$\Delta S^0/\Delta N^0$	0.56
Effective bulk lifetime	30 ns
Surface lifetime	4 ns

times larger than the wavelength, the limiting case equations (20) and (22) for slowly varying $\Delta\epsilon$ are used in this example. Substitution of the grating excitation initial conditions into Eqs. (20) and (22) and integration yield four different time-dependent diffraction efficiencies. Figure 4 gives the calculated diffraction signals after normalization of the diffraction efficiency to the largest signal for each of the possible probe geometries. The constants used in the calculation are representative of the material constants of the anthracene sample used for the data shown in Fig. 3 and are given in Table 1. The only adjustable parameter is the ratio of excited states to strain amplitudes, $\Delta N^0/\Delta S^0$. This parameter, adjusted to correct the relative size of the acoustic oscillations and the excited-state signal for the transmission case data (Fig. 3a), is held constant for the two reflection cases.

The two transmission cases shown in Figs. 4a and 4b are virtually identical, since the surface contributions, which are not identical, are more than 1 order of magnitude smaller than the bulk contribution to the signal. As we discussed in Section 3, the bulk contribution is identical for either probe direction, since the bulk contribution is an equal spatial weighting of the bulk dielectric modulation.

The reflection geometry gives significantly different results. While the signals in Figs. 4a and 4b decay slowly with the bulk excited-state lifetime, those in Figs. 4c and 4d decay rapidly with the surface lifetime. As is also seen in the experimental data, the reflection signal with a front incident probe (Fig. 4c) has far less of an acoustic component relative to the case of the back incident probe (Fig. 4d). Both reflection geometries are surface selective, but the excitation beams that are incident upon the front side create more surface states on the front side. Thus the relative magnitudes of the excited-state to acoustic contribution for front and back incident reflected diffracted beams are qualitatively correct, and the calculation reproduces the essential features of the data.

5. CONCLUDING REMARKS

The transmitted diffraction signal has a bulk contribution that prevails if the sample is thick (greather than a wavelength). This is the case that has commonly been explored in the laboratory. For thick samples the reflection and transmission signals look at fundamentally distinct regions of the sample. This was illustrated in the experiments presented above. Reflection and transmission gratings gave dramatically different time-dependent signals both in theory and in practice. By analyzing various probe configurations of a transient grating experiment, one can extract additional information on the spatial distributions of the index perturbations that is not available from a single experimental geometry.

Probing the surface with transient grating experiments has some similarity to surface-selective second-harmonic generation. Both depend on an abrupt change in the dielectric function to produce surface selectivity. The transient grating experiment is readily applicable to the study of dynamics on surfaces on fast and slow time scales. Although it was not explicitly discussed in this paper, surface reflection gratings can also be used in surface nonlinear spectroscopy. For example, by fixing the probe delay time and the excitation wavelength and tuning the wavelength of the probe beam, one should be able to obtain a surface excited state–excited state spectrum. The development in this paper of the appropriate theoretical description of reflection and transmission transient grating experiments, demonstrating the ability to measure the surface dynamic and spectroscopic properties of materials, can have many important applications.

The theoretical treatment presented in this paper shows that reflection geometry of diffraction exclusively probes the surface in situations in which the modulation of the dielectric constant varies slowly relative to a wavelength of light in the direction normal to the grating wave vector. This is a type of sample that is commonly en-

countered. Equation (20) describes the case. If, however, the dielectric constant changes quickly relative to the wavelength, then the more general Eq. (19) must be utilized. For some materials of interest, such as multiquantum-well structures, there can be boundaries or interfaces inside the sample that cause jumps in the dielectric function. In such a case diffraction can occur from each interface. This could be theoretically treated by a generalized solution of Eq. (18) for multiple interfaces. The important point is that in a simple sample the reflection signal will come from the surface or the interface. This leads to a powerful new method of analysis for transient grating diffraction in which bulk and surface effects can be measured separately. Similar considerations apply to many types of four-wave mixing experiments, such as photon echoes and coherent anti-Stokes Raman scattering. The theory presented above can readily be extended to those experiments.

ACKNOWLEDGMENTS

The authors are grateful to J. Keller for clarification of mathematical details. This study was supported by the National Science Foundation, Division of Materials Research (grant DMR87-18959). Additional support was provided by the Office of Naval Research (grant N00014-89-J1119). I.M. Fishman acknowledges the support of the Medical Free Electron Laser Program, Office of Naval Research (grants N00014-89-K0154 and N00014-86-K0118).

*Permanent address, DuPont Corporate Research and Development, Experimental Station 328/204, Wilmington, Delaware 19880.

REFERENCES

1. H. J. Eichler, P. Gunter, and D. W. Pohl, *Laser Induced Dynamic Gratings* (Springer-Verlag, Berlin, 1986).
2. P. D. Hyde, T. E. Evert, and M. D. Ediger, J. Chem. Phys. **93,** 2274 (1990).
3. D. McMorrow, W. T. Lotshaw, and G. A. Kenney-Wallace, IEEE J. Quantum Electron. **24,** 443 (1988).
4. F. W. Deeg, S. R. Greenfield, J. J. Stankus, V. J. Newell, and M. D. Fayer, J. Chem. Phys. **93,** 3503 (1990).
5. R. Trebino, C. E. Barker, and A. E. Siegman, IEEE J. Quantum Electron. **QE-22,** 1413 (1986).
6. S. Ruhman, B. Kohler, A. G. Joly, and K. A. Nelson, IEEE J. Quantum Electron. **24,** 470 (1988).
7. L. Genberg, Q. Bao, S. Gracewski, and R. J. D. Miller, Chem. Phys. **131,** 81 (1989).
8. T. S. Rose, R. Righini, and M. D. Fayer, Chem. Phys. Lett. **106,** 13 (1984).
9. J. M. Brown, L. J. Slutsky, K. A. Nelson, and L.-P. Cheng, J. Geophys. Res. **94,** 9485 (1989).
10. T. Dreier and D. J. Rakestraw, Appl. Phys. B **50,** 479 (1990).
11. J. T. Fourkas, T. R. Brewer, H. Kim, and M. D. Fayer, Opt. Lett. **16,** 177 (1991).
12. I. Abella, N. A. Kurnit, and S. R. Hartmann, Phys. Rev. **141,** 391 (1966).
13. S. R. Hartmann, Sci. Am. **128,** 32 (1968).
14. L. R. Narasimhan, K. A. Littau, D. W. Pack, Y. S. Bai, and M. D. Fayer, Chem. Rev. **90,** 439 (1990).
15. M. Berg, C. A. Walsh, L. R. Narasimhan, K. A. Littau, and M. D. Fayer, J. Chem. Phys. **88,** 1564 (1988).
16. L. Schultheis, J. Kuhl, A. Honold, and C. W. Tu, Phys. Rev. Lett. **57,** 1797 (1986).
17. E. O. Gobel, K. Leo, T. C. Damen, J. Shah, S. Schmitt-Rink, W. Schafer, J. F. Muller, and K. Kohler, Phys. Rev. Lett. **64,** 1801 (1990).
18. Y. R. Shen, *The Principles of Nonlinear Optics* (Wiley, New York, 1984), Chap. 25, and references therein.
19. K. A. Nelson, R. Casalegno, R. J. D. Miller, and M. D. Fayer, J. Chem. Phys. **77,** 1144 (1982).
20. R. Collier, L. B. Burkhardt, and L. H. Lin, *Optical Holography* (Academic, New York, 1971), Chap. 9.
21. H. Kogelnik, Bell Syst. Tech. J. **48,** 2909 (1969).
22. J. S. Meth, C. D. Marshall, and M. D. Fayer, Solid State Commun. **74,** 281 (1990).
23. C. D. Marshall, I. M. Fishman, and M. D. Fayer, Phys. Rev. B **43,** 2696 (1991).
24. K. A. Kong, J. Opt. Soc. Am. **67,** 825 (1977), and references therein.
25. M. Born and W. Wolf, *Principles of Optics,* 4th ed. (Pergamon, Oxford, 1970).
26. N. Bloembergen, *Nonlinear Optics* (Benjamin, Reading, Mass., 1965).
27. M. D. Fayer, IEEE J. Quantum Electron. **QE-22,** 1437 (1986).
28. J. S. Meth, C. D. Marshall, and M. D. Fayer, J. Appl. Phys. **67,** 3362 (1990).
29. J. S. Meth, C. D. Marshall, and M. D. Fayer, Chem. Phys. Lett. **162,** 306 (1989).
30. B. A. Auld, *Acoustic Fields and Waves in Solids* (Wiley, New York, 1973), Vol. 2.